

A Statistical–Dynamical Parameterization of Interception and Land Surface–Atmosphere Interactions

JORGE A. RAMÍREZ

*Water Resources, Hydrologic and Environmental Sciences Division, Civil Engineering Department,
Colorado State University, Fort Collins, Colorado*

SHARIKA U. S. SENARATH

Civil and Environmental Engineering Department, University of Connecticut, Storrs, Connecticut

(Manuscript received 18 November 1997, in final form 2 July 1999)

ABSTRACT

At a local scale, the interception capacity of the canopy depends on a variety of climatic and canopy factors. Of particular importance is the intensity of rainfall—interception capacity varies inversely with rainfall intensity. At a field or regional scale, like the scale of global climate models, the spatially averaged interception also depends significantly on the spatial variability of rainfall intensity and total precipitation depth.

A new parameterization of canopy interception is developed. In the new parameterization, the spatial average of actual interception is obtained as a function of rainfall intensity and total precipitation depth, and of an interception capacity, which depends on the characteristics of the leaf surface and of the vegetation cover. In a statistical–dynamical framework, the new parameterization also accounts for the subgrid-scale spatial variability of rainfall intensity and total precipitation depth.

The implications of accounting for the dependence of interception capacity on rainfall characteristics are examined by assessing the consequent responses of the energy and the water fluxes at the land surface. This is accomplished by incorporating the new parameterization into a soil–plant–atmosphere column model that is fundamentally based on the physical parameterizations of NCAR’s Community Climate Model.

1. Introduction

Interception, that is, the depth of rainwater retained on a forest or litter canopy for subsequent evaporation, constitutes a significant portion of the incident precipitation in certain watersheds (Calder 1977, 1992), and has a significant influence on the energy and water budgets at the land surface.

Interception capacity (generally expressed in units of volume per unit area) refers to the maximum volume of water that can be stored on the projected storage area of the vegetation—that is, on the area of leaves, twigs, and branches that can retain water against gravity—under still air conditions (Horton 1919). Interception capacity is influenced by factors such as leaf area, leaf area index, precipitation intensity, and surface tension forces resulting from leaf surface configuration, liquid viscosity, and mechanical activity (e.g., Aston 1979).

The forces associated with intense rainfall have the

capability of dislodging previously intercepted water and reducing the interception capacities of foliage surfaces by a substantial amount. “Trimble and Weitzman (1954) attribute greater summer throughfall during high intensity rain to previously intercepted water being physically beaten from downward sloping leaves” (Helvey and Patric 1965). Bultot et al. (1972) and Wells and Blake (1972) have shown that interception and rainfall intensity are inversely related to each other. For a *Pinus radiata* forest in Whakarewarewa in New Zealand, Wells and Blake (1972) have observed an increase in interception during the early part of the storm, and a subsequent decrease in interception with increasing intensity. Figure 1 illustrates the relationship between the percentage interception and storm depth for four different rain rate values and ranges. Franken et al. (1982) observed similar results after analyzing data obtained from a study site in the Amazon rainforest. For an old-growth Douglas fir [*Pseudotsuga menziesii* (Mirb.) Franco] canopy in Oregon, Massman (1983) observed a clear dependence of interception on rainfall intensity and identified it as one of the main contributors toward the drip of intercepted rainwater.

However, in most current GCM land surface schemes,

Corresponding author address: Dr. Jorge A. Ramírez, Department of Civil Engineering, Colorado State University, Fort Collins, CO 80523-1372.

E-mail: ramirez@engr.colostate.edu

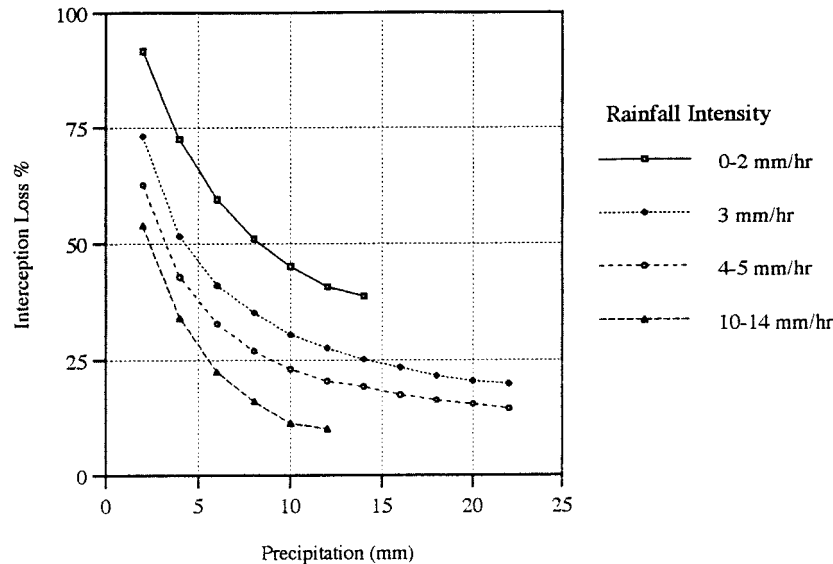


FIG. 1. Plot of percentage interception vs rainfall depth under varying intensities (adopted from Wells and Blake 1972).

interception is prescribed as a function of seasonal leaf area index (LAI) and fractional vegetation cover with little regard for rainfall intensity (e.g., Dickinson et al. 1986; Sellers et al. 1986, 1996). Many researchers have highlighted the inadequacy and the deficiency of modeling interception as independent of rain rate (e.g., Jackson 1975; Massman 1980, 1983). It is equally important to account for the subgrid-scale spatial variability of rain properties. In GCM land surface parameterizations that do not account for this variability, interception tends to be overestimated when compared with observations (Lean and Warrilow 1989; Shuttleworth 1988). The importance of accurately accounting for interception has been reemphasized in the Project for Intercomparison of Land-surface Parameterization Schemes phase 1c, as a necessary prerequisite for improved climate simulations (Koster and Milly 1997).

2. Objectives and general approach

In this study, interception capacity is modeled as a decreasing function of a spatially variable rainfall intensity and as a function of the characteristics of the leaf surface and of the vegetation cover. Actual interception is modeled as a nonlinear function of interception capacity and precipitation depth. Furthermore, the grid-average volume of actual interception is derived in a *statistical-dynamical* framework, so that the subgrid spatial variability of rainfall intensity and total precipitation depth are explicitly taken into account using probability density functions (pdfs).

The implications of accounting for the dependence of interception capacity on rainfall intensity are examined by incorporating the new interception parameterization into the soil-plant-atmosphere column model of Ra-

mírez (1991) and by assessing the consequent responses of the energy and the water fluxes at the land surface. Two *standard* land surface schemes present in the column model are modified to include the new interception parameterization, namely the Biosphere-Atmosphere Transfer Scheme (BATS) of Dickinson et al. (1986) and the statistical-dynamical parameterization of Entekhabi and Eagleson (1989).

3. Interception parameterization

a. Interception capacity

A strong dependence exists between interception capacity and rainfall intensity (e.g., Massman 1983; P.S. Eagleson 1980, personal communication; Aston 1979). Canopies register large interception under misty, drizzle-like conditions with light intensities, and small interception under intense precipitation conditions (Bultot et al. 1972; Wells and Blake 1972). As with many other choices in developing models and parameterizations, the actual choice of the form of this dependence is a matter of (physically based) mathematical convenience. Two different representations are defined here. One assumes an exponential decay of interception capacity with rainfall intensity,

$$h_o(i) = ae^{-ci}, \quad i \geq 0 \quad (1a)$$

the other assumes a simple linear decay (e.g., P. S. Eagleson 1980, personal communication),

$$h_o(i) = \begin{cases} a - bi, & 0 \leq i \leq a/b \\ 0, & i > a/b, \end{cases} \quad (1b)$$

where h_o is interception capacity (m); i is precipitation rate (m s^{-1}); a is maximum dew depth (m); and b and

c are constants. The maximum dew depth, a , of Eq. (1) depends only on the vegetative characteristics of the canopy and constitutes an upper limit to the interception capacity; the constants b and c depend on both vegetative and climatic conditions and characterize the rate of decay of interception capacity with rainfall intensity. The interception capacity is estimated as the absolute value of the intercept of the regression line of a plot of net rainfall against gross rainfall data. Using this methodology, Crockford and Richardson (1990) obtained interception capacity values of 1.7 mm and 2 mm for a eucalyptus forest and a pine plantation in the upper Yass Basin in Australia. Zinke (1967) found interception capacity values ranging from 0.25 to 9.14 mm for trees and suggested an approximate mean interception capacity of 1.3 mm for most grasses, shrubs, and trees.

Rainfall intensity is a spatially variable quantity whose variability can be described with the one-parameter exponential pdf (e.g., Eagleson 1978; Ramírez and Bras 1985; Entekhabi and Eagleson 1989),

$$f_I(i) = \alpha e^{-\alpha i}, \quad i \geq 0, \quad (2)$$

where α is the reciprocal of average precipitation intensity over the wetted fraction of the surface, $s \text{ m}^{-1}$. If the mean precipitation intensity over the grid square is $1/\alpha^*$ (e.g., as might be obtained from a GCM), then the mean precipitation intensity over the wetted fraction

is $1/\alpha = 1/(\alpha^* \sigma_w)$, and σ_w is the fraction of the surface that is wetted. Therefore, through this procedure, the distribution of Eq. (2) accounts for the effects of fractional coverage by precipitation events, in the manner of Entekhabi and Eagleson (1989). Using Eq. (2) and a *derived distribution* approach, the pdf of interception capacity is obtained in the appendix.

b. Actual interception

The amount of precipitation that is actually intercepted by the canopy, h_a , is equal to the total precipitation depth, h , when interception capacity exceeds total precipitation depth, or equal to the interception capacity otherwise. Precipitation depth and interception capacity are spatially variable quantities whose variability can be described with probability density functions. In addition to the pdf of interception capacity derived in the appendix, a two-parameter gamma probability density function for precipitation depth is assumed in this analysis. The two-parameter gamma pdf provides a good fit over a wide range of climatic types, is analytically tractable, and is widely used to represent precipitation depths (e.g., Ison et al. 1971; Eagleson 1978).

The spatial average of normalized actual interception, $E[h_a^*]$, is obtained in the appendix for each of the two modeling options. The resulting functions are

$$E[h_a^*] = \int_0^1 \left\{ \eta P\left(\kappa + 1, \frac{\kappa h_o^*}{\eta}\right) + h_o^* \left[1 - P\left(\kappa, \frac{\kappa h_o^*}{\eta}\right) \right] \right\} \tau h_o^{*(\tau-1)} dh_o^* \quad (3a)$$

for the exponential model; and

$$E[h_a^*] = \int_0^1 \left\{ \eta P\left(\kappa + 1, \frac{\kappa h_o^*}{\eta}\right) + h_o^* \left[1 - P\left(\kappa, \frac{\kappa h_o^*}{\eta}\right) \right] \right\} \nu e^{-\nu(1-h_o^*)} dh_o^* \quad (3b)$$

for the linear model, respectively.

In the above equations, $P(\cdot)$ denotes Pearson's incomplete Gamma function; κ and $\lambda = \kappa/m_H$ (m^{-1}) are the parameters of the pdf of precipitation depths; m_H is mean precipitation depth (m); $h_a^* = h_a/a$ is normalized actual interception; $h_o^* = h_o/a$ is normalized interception capacity; and $\eta = \kappa/(\lambda a)$ is a climate-vegetation parameter equal to the ratio of mean precipitation depth to maximum dew depth. The normalized interception capacity decay parameter of the exponential model is $\tau = 1/E(i)c = \alpha/c$, and that of the linear model is $\nu = (a/b)/E(i) = \alpha a/b$. The larger τ and ν , the slower the decay rate of interception capacity with rain intensity and the larger the expected value of actual interception.

Figures 2a and 2b present the pdf of normalized *interception capacity* for the exponential and linear models, respectively. The probability mass at the origin of

the linear model, and the magnitude of $f_{H_o}(h_o) dh_o$ of the exponential model near the origin increase as the rate of decay increases. This occurs for mean rainfall intensities that are large compared to a/b , or to $1/c$. For the linear model for example, as the decay rate increases (i.e., as the mean rainfall intensity increases) the pdf tends toward a uniform distribution between 0 and 1 with a density of probability approaching ν , and the probability mass at the origin approaching $(1 - \nu)$. That is, the probability that the interception capacity is zero increases as ν decreases. As the mean intensity decreases, or as the rate of decay decreases, or as the decay parameter increases as would happen either for increasing a or decreasing b , the probability that the rainfall would remove all of the retained water from the leaves decreases, and the distribution of probability density behaves more like a positive exponential function, a

Probability Density Function of Normalized Surface Interception Capacity

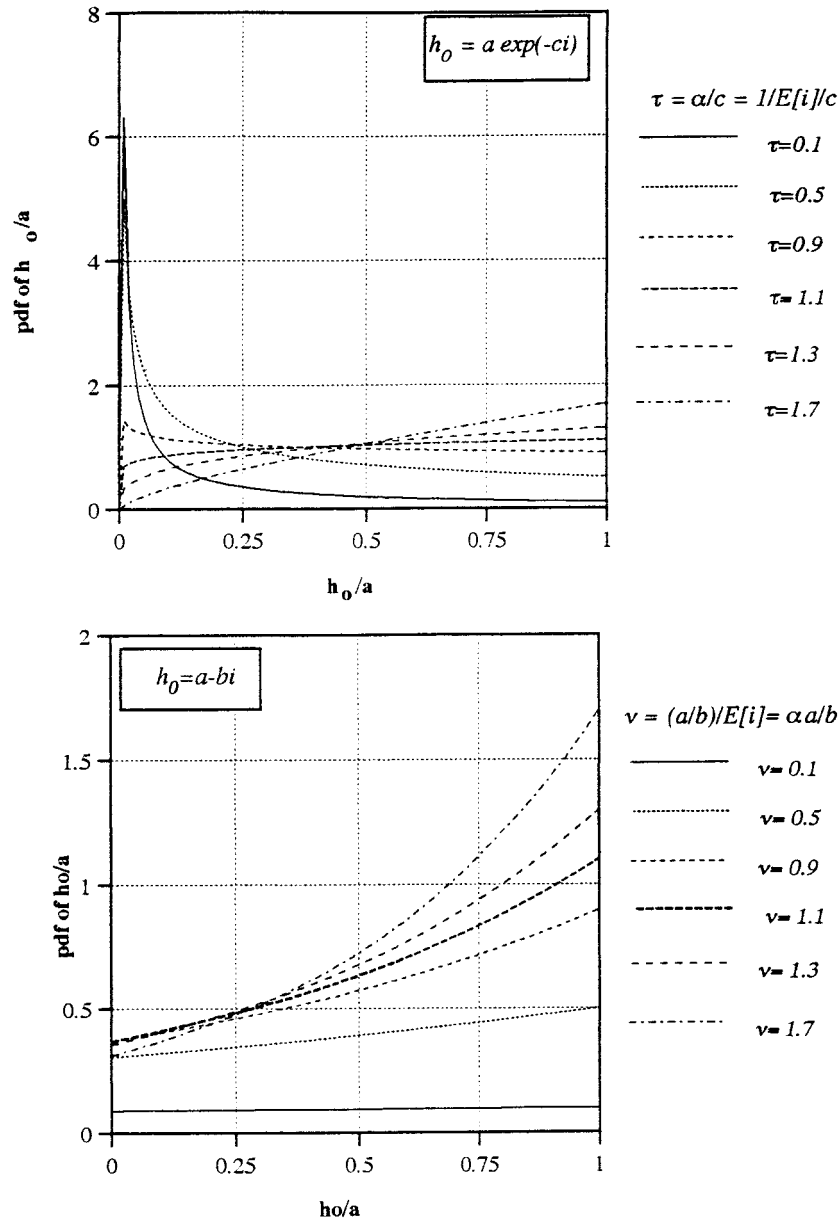


FIG. 2. (a) Derived probability density function of normalized canopy interception capacity for the exponential model. (b) Derived probability density function of normalized canopy interception capacity for the linear model.

monotonically increasing function of the normalized interception capacity. That is, the likelihood of having normalized interception capacities approaching unity increases. This interpretation of the behavior of the linear model can be extended in an analogous manner to the exponential model.

Figures 3a and 3b show the variation of the average actual interception as a function of the rate of decay of interception capacity, for different values of the climate-

vegetation parameter η and the shape parameter of the distribution of precipitation depths. For both models, as the decay parameter increases (i.e., as the rate of decay decreases), the average actual interception increases. This increase is faster for the exponential model, especially at low values of the decay parameter. Also, as the value of the climate-vegetation parameter increases, that is, as the mean rainfall depth becomes large with respect to the maximum canopy dew depth, the average

Expected Value of Normalized Actual Interception

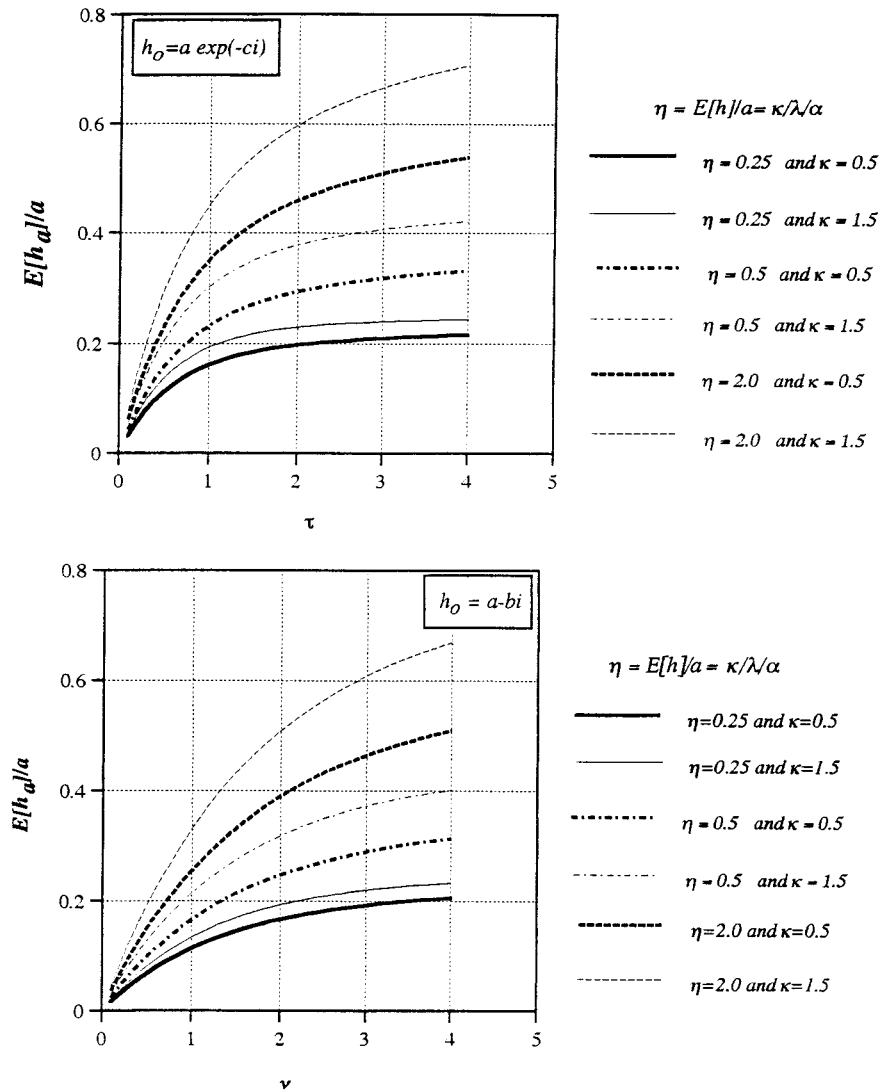


FIG. 3. (a) Expected value of normalized actual interception—exponential model. (b) Expected value of normalized actual interception—linear model.

of the actual interception increases, as expected. However, the rate of increase decreases as η gets larger, as the actual interception is limited by the maximum dew depth. For low values of the climate-vegetation parameter, that is, when the mean rainfall depth is small relative to the maximum canopy dew depth, the effect of the shape of the distribution of precipitation depths is not as large as for high values of the climate-vegetation parameter. For low values of η , the actual interception is supply limited, and changes in actual interception will result primarily from changes in the interception capacity, that is, changes in the decay parameter. This assessment is valid for both the exponential and linear models. Finally, Figs. 4a and 4b illustrate the dependence of average actual interception (as a fraction of

average precipitation depth) on rainfall intensity and total precipitation depth. As expected, the average actual interception decays as both rainfall intensity and total precipitation depth increase. Of particular importance for verification is to note the striking similarity of Figs. 4a and 4b with Fig. 1.

Compiling comprehensive databases of values for a , b , and c for a variety of climatic conditions and species types is a prerequisite for making use of this parameterization. Procedures like those used by Crockford and Richardson (1990) can be used to estimate a , while the procedure of Wells and Blake (1972) leading to Fig. 1 can be used to obtain estimates of b and c for a variety of climatic conditions and species types. Similarly, in order to be able to use this parameterization in GCMs,

Mean Actual Interception Loss as a Fraction of Mean Total Storm Depth

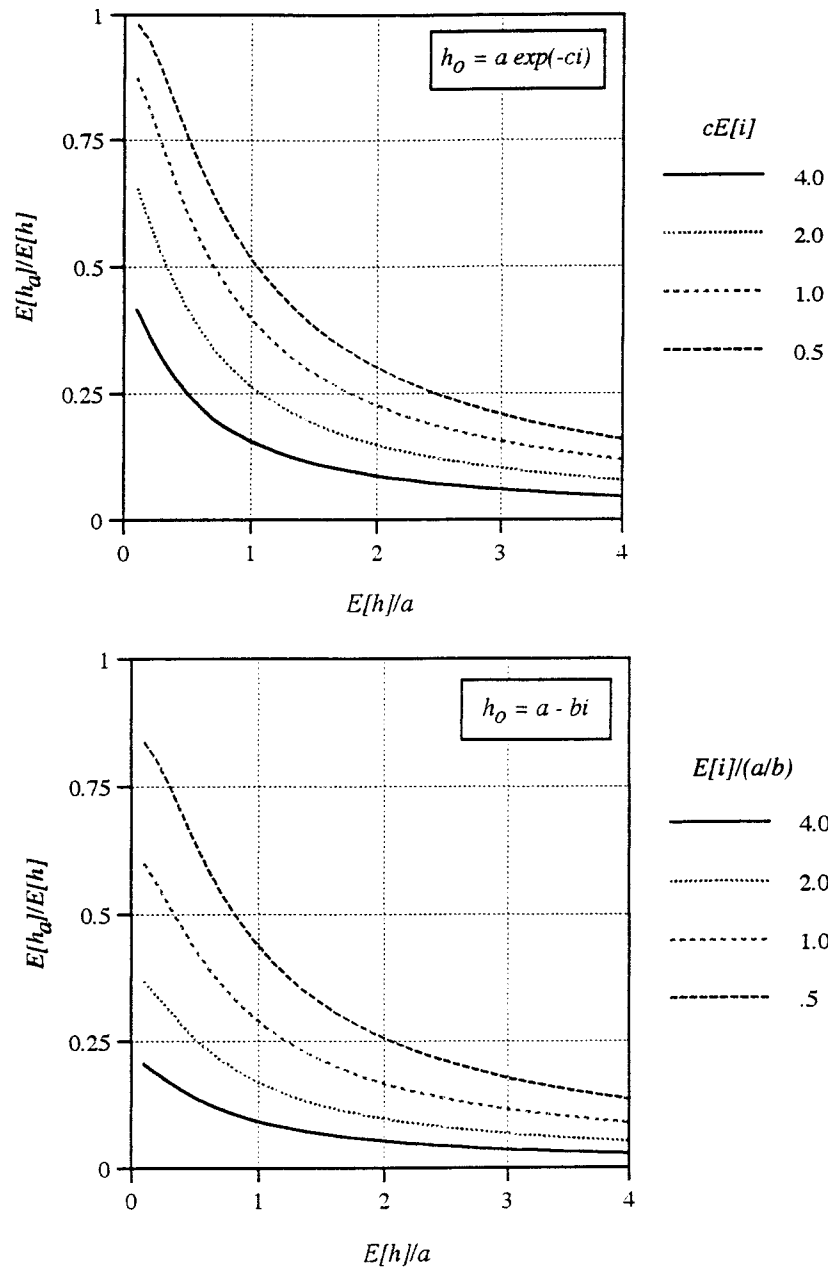


FIG. 4. (a) Expected value of actual interception as a fraction of expected precipitation depth—exponential model. (b) Expected value of actual interception as a fraction of expected precipitation depth—linear model.

a global climatology of storm rainfall characteristics α , λ , and κ must be developed. This can be achieved in the manner of Hawk and Eagleson (1992).

4. Big leaf option

The soil–plant–atmosphere column model (Ramírez 1991) is composed of coupled atmospheric and land

surface modules. The atmospheric module includes moist-convective and stable condensation adjustments, cloud and radiative parameterizations, and vertical diffusion processes, whose parameterizations are those of NCAR’s Community Climate Model [see Williamson et al. (1987) for more details]. The land surface module is designed to be optional from three alternatives: (a) a simple parameterization of hydrology based on the so-

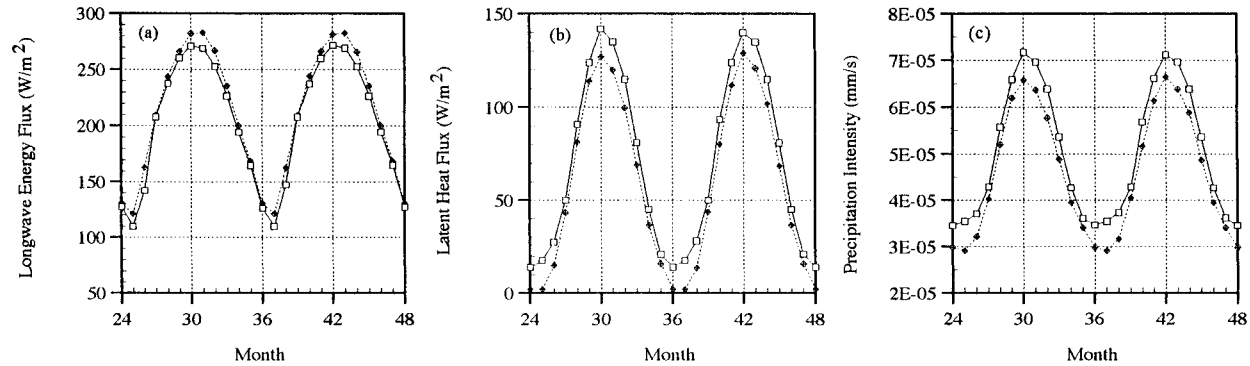


FIG. 5. Seasonal distribution of surface fluxes generated with the big-leaf option of the column model (BATS, solid; new parameterization, dotted).

called *bucket hydrology*; (b) a more complex parameterization based on the BATS (Dickinson et al. 1986) scheme; and (c) a statistical–dynamical representation of the land surface hydrology that accounts explicitly for the subgrid-scale variability of several land surface and climatic characteristics, including the effects of partial wetting by storms. Model forcing is in the form of incoming solar radiation at the top of the column and seasonal cycles of lateral heat and moisture convergences.

The *big-leaf* option of column model is an extended version of the BATS land surface scheme (Ramírez and Genovez 1994). However, the interception capacity parameterization in BATS is independent of rain rate, and assumes that no drip occurs until the canopy is fully saturated. This and other limitations of BATS have been related by several investigators to inadequacies in the simulation of interception. In a land use change study conducted by Dickinson and Henderson-Sellers (1988) using BATS, they showed that interception is overestimated. Eltahir and Bras (1993) have related this mismatch to the lack of sufficient parameterization to represent the subgrid-scale spatial variability of rainfall, and to the crude, deterministic interception parameterization. The parameterization of interception capacity as independent of rainfall intensity is another reason for this overestimation. Consequently, in this paper the big-leaf option is modified by incorporating the linear version [Eq. (1b)] of the interception parameterization developed above.

5. Results

Seasonal distributions of several hydrologic and energy fluxes obtained from column model simulations with the original BATS model and with the modified BATS model, which includes the new interception parameterization, are compared. A 30-minute time step is used for all simulations. The simulated differences are strictly due to changes brought forth by modeling interception capacity as a decreasing function of rain rate. For all simulations, an evergreen needle-leaf tree forest

with a canopy cover of 80% is selected. The soil and vegetation parameter values used for the simulations correspond exactly to those of BATS for an evergreen needle-leaf forest (Dickinson et al. 1986).

a. Longwave energy flux

Accounting for the dependence of interception capacity on rainfall intensity induces an increase of the longwave flux as shown in Fig. 5a. Dependence on rainfall intensity leads to a decrease of interception capacity, which in turn leads to a decrease in actual interception volumes. The consequent reduction in canopy evaporation induces an increase in temperature and hence an increase in longwave flux.

b. Latent heat energy fluxes

As a result of the decreased interception capacity, the amount of canopy water available for evaporation, and hence canopy evaporation (which takes place at potential rates) decrease as shown in Fig. 5b. The increased contribution of water falling on the ground gives rise to an increase in soil moisture and surface runoff. However, soil moisture is below saturation during most of the year and bare-soil evapotranspiration is under soil control and occurs at subpotential rates. Consistent with this latent heat flux decrease, sensible heat fluxes increase.

c. Precipitation intensity

As the dependence of interception capacity on rainfall intensity increases, precipitation intensity decreases (Fig. 5c). Smaller interception volumes give rise to smaller evaporative contributions from interception (see Fig. 5b) and larger contributions to soil moisture storage and surface runoff, and thus to a smaller volume of water vapor in the atmosphere.

TABLE 1. Percent change of water in upper soil layer and surface runoff. The change refers to the difference between the new parameterization and the standard BATS model.

Month	% Δ Soil moisture <i>b</i>		% Δ Surface runoff <i>b</i>	
	3600	10 800	3600	10 800
1	0	0	0	0
2	0.5	-4.46	3.61	10.89
3	0.43	2.17	6.99	69.09
4	1.33	3.54	38.91	118.18
5	2.24	5.83	66.11	190.38
6	3.17	7.69	77.58	236.32
7	2.7	7.66	86.41	260.68
8	1.78	5.78	55.6	198.28
9	0.88	4.39	18.44	124.47
10	0	1.72	4.6	52.3
11	0.22	0.66	0.5	8.15
12	-0.73	-0.59	-0.6	-0.3

d. Soil moisture and surface runoff

Accounting for the dependence of interception capacity on rainfall intensity induces an increase in soil moisture content in the upper soil layer during late spring, summer, and early fall. This in turn leads to an increase in surface runoff during most of the year. Lower interception gives rise to larger net precipitation at the surface, and hence to higher soil moisture contents and larger surface runoff rates. Although the rainfall intensities decrease during the colder months of the year, the runoff rates are high due to the presence of ground freezing temperatures as well as high soil moisture contents. The seasonal percentage changes of soil moisture and surface runoff rates between the standard BATS and the new interception parameterization are given in Table 1. For comparison purposes, results corresponding to several values of *b* are presented.

6. Statistical dynamical option

The original statistical-dynamical land surface option of the climate model is based on that of Entekhabi and Eagleson (1989), which contains no interception parameterization and which includes only two parameters to represent vegetation: 1) the wilting matric potential and 2) the fractional vegetation cover, which is assumed constant during the growing season. The modifications detailed in the following sections address some of these issues.

a. Interception parameterization

Considering an inverse linear dependence of interception capacity on rainfall intensity [Eq. (1)], the grid average actual interception volume of Eq. (3b) is incorporated into the statistical-dynamical option.

b. Fractional vegetation cover

Two widely used fractional vegetation cover parameterizations are implemented that take into account the intraseasonal variability of vegetation cover. The first does so by modeling fractional vegetation cover as a function of LAI; the second as a function of ground temperature.

Mahfouf and Jacquemin (1989) and Lee (1992) have used the following empirical relationship for fractional vegetation cover, σ_f ,

$$\sigma_f = 1 - e^{-\mu \text{LAI}}. \quad (4)$$

Mahfouf and Jacquemin (1989) have assumed μ to be equal to 0.8. However, Lee (1992) has used a value of 0.75. The latter agrees well with the First ISLSCP (International Satellite Land-Surface Climatology Project) Field Experiment (FIFE) observational data (Sellers et al. 1988), and hence can be used with a high degree of confidence for grass land-types. Therefore, in this study, Eq. (4) with a μ of 0.75 is used for grass land-types. LAI is parameterized as in Dickinson et al. (1986),

$$\text{LAI} = \text{LAI}_{\min} + F(T_g)(\text{LAI}_{\max} - \text{LAI}_{\min}). \quad (5)$$

For other vegetation and land-cover classes the fractional vegetation cover is formulated as the following function of ground temperature (Dickinson et al. 1986),

$$\sigma_f = \begin{cases} \sigma_{f,\text{Summer}}, & T_g > 298 \text{ K} \\ \sigma_{f,\text{Summer}} - \Delta\sigma_{f,\text{Seasonal}}, & T_g < 273 \text{ K} \\ \sigma_{f,\text{Summer}} - [1 - F(T_g)]\Delta\sigma_{f,\text{Seasonal}}, & 273 \text{ K} \leq T_g \leq 298 \text{ K}, \end{cases} \quad (6)$$

where $F(T_g) = 1 - [0.0016(298 - T_g)^2]$. Dickinson et al. provided a complete set of values for the maximum fractional vegetation cover ($\sigma_{f,\text{Summer}}$) and the difference in seasonal cover ($\sigma_{f,\text{Seasonal}}$) for each of the vegetation/land-cover types above.

c. Foliage variable modification

In the new parameterization the maximum dew depth *a* is formulated as follows:

$$a = \gamma^*(\text{LAI} + \text{SAI}). \quad (7)$$

The maximum and minimum LAI values, as well as the stem area index (SAI) values for all vegetation types are provided in Dickinson et al. The maximum depth of water per unit leaf and stem area indices is γ^* . A value of 0.2 mm for γ^* is used in BATS. However, Hancock and Crowther (1979) have found 0.25 mm per unit LAI to be a more representative value for conifers. Sellers et al. (1989) in the process of calibrating SiB predictions with Amazonian rainforest data have found 0.1 mm to be more representative for nonconifers. In this work, values of 0.1, 0.25, 0.2 mm are used to rep-

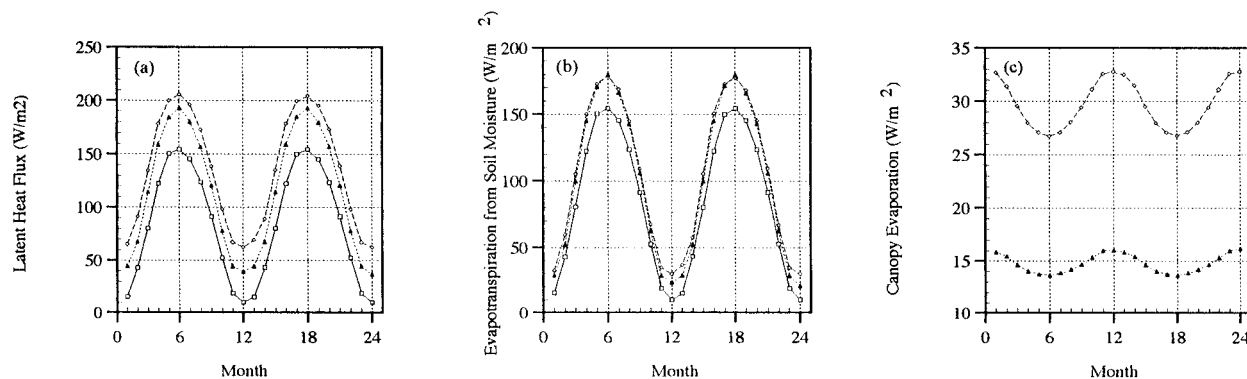


FIG. 6. Seasonal distribution of latent heat fluxes generated with the statistical–dynamical option of the column model [original (no interception), solid; new (tall grass), dotted; new (evergreen broadleaf), dashed].

represent the maximum dew-depth for nonconifer trees, conifer trees, and grasses, respectively.

Finally, the fraction of leaves covered by intercepted water is obtained in the manner of Deardoff (1978) as

$$\rho^* = \left[\frac{E[h_a]}{a} \right]^{2/3}, \quad (8)$$

where $E[h_a]$ is the expected value of the actual interception [Eq. (3b)], and a is the maximum dew depth.

7. Results

Several simulations are compared corresponding to the following cases:

- 1) a simulation using the original statistical–dynamical parameterization (i.e., without any interception parameterization);
- 2) a simulation using the new statistical–dynamical interception parameterization for a tall grass vegetation type (hereafter referred to as TG); and
- 3) a simulation using the new statistical–dynamical interception parameterization for an evergreen broadleaf vegetation type (hereafter referred to as EB).

Except as indicated above, the soil, climate, and vegetation parameter values used for the simulations correspond exactly to those of BATS for the two land covers simulated and to those of Entekhabi and Eagleson (1989) for a clay soil. A fractional vegetation cover of 0.8 and a wilting matric potential of -200 m are used in the original model simulation run. The time step used for the three simulations is equal to 30 min.

a. Latent heat flux

With the introduction of the new interception parameterization, the latent energy fluxes increase significantly (Fig. 6a). On the average, the magnitude of the response of EB to the modification is larger than that of TG. Also more and less pronounced deviations are evident between EB and TG during winter and summer

months, respectively. Consistent with this, sensible heat fluxes decrease.

b. Evapotranspiration from soil moisture

In response to the modification, evapotranspiration increases significantly for EB and TG vegetation types. This is expected as the new parameterization allows for contributions from transpiration, which takes place at near-potential rates. During the colder months due to the reduced precipitation and energy availability, and differences in LAI and fractional vegetation cover between the two vegetation types, the differences in evapotranspiration from soil moisture among the three (original, TG, and EB) are more pronounced. During the warmer months of the year due to the maximization of the canopy cover, the differences between the two vegetation types are less significant, although they are significant when compared to the original parameterization. These results are illustrated in Fig. 6b.

c. Canopy evaporation

In the original version of the model, due to the omission of interception, the canopy evaporation is always zero. Since LAI is larger for EB throughout the annual cycle, the EB simulation shows a higher canopy evaporation than TG. During the warmer months, due to the maximization of the canopy cover in both land types, the differences in canopy evaporation between TG and EB land uses are less pronounced. Since interception capacity is modeled as a decreasing function of rainfall intensity, with the increase of rainfall intensities the canopy evaporation is also relatively lower for both land uses during the summer months. The results are shown in Fig. 6c.

d. Precipitation intensity

As illustrated in Fig. 7a, the new parameterization gives rise to an increase in rainfall intensity. Actual

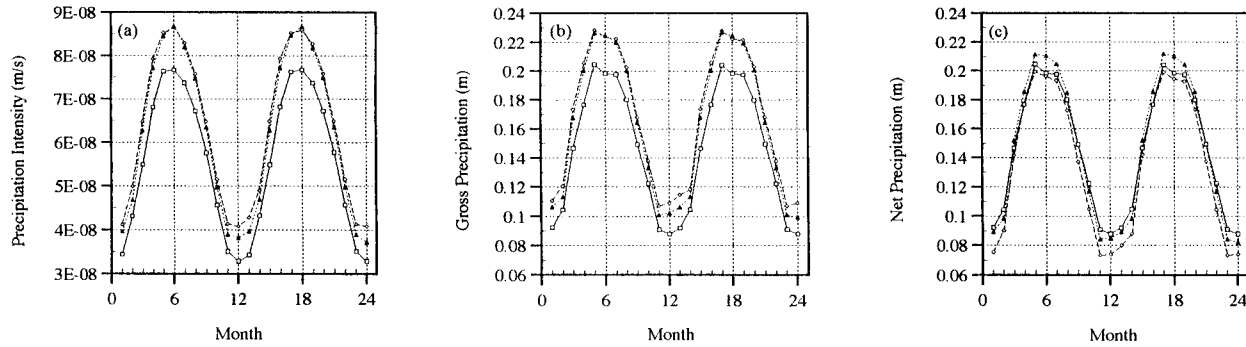


FIG. 7. Seasonal distribution of precipitation generated with the statistical–dynamical option of the column model [original (no interception), solid; new (tall grass), dotted; new (evergreen broadleaf), dashed].

interception gives rise to increases in the evaporative contribution from the foliage. That, in turn, leads to an increase in the atmospheric moisture content, and hence to an increase in precipitation intensity. The seasonal percentage change of precipitation intensity for both EB and TG is given in Table 2.

e. Gross precipitation

Gross precipitation depths increase significantly especially during the warmer months of the year. Gross precipitation in EB is larger than in TG, on average. EB contributions from both canopy evaporation and evapotranspiration from soil moisture are higher than those of TG. Therefore, EB produces larger precipitation intensities and depths. Results are shown in Fig. 7b.

f. Net precipitation

With respect to the original model, there is a decrease in net precipitation for most of the year for the TG simulation, and throughout the year for the EB simulation (see Fig. 7c). However, the new parameterization also gives rise to an increased release of water back into the atmosphere, and during the summer months (March–August) in TG landmasses, this offsets the reductions in net precipitation due to interception. During the sum-

mer months since rain rates are high, interception values decrease substantially in both TG and EB.

g. Soil moisture and surface runoff

The interception modification leads to a significant decrease in soil moisture contents in EB and TG during most of the year (see Fig. 8) since a significant amount of the incident precipitation never reaches the ground. During the winter months, soil moisture reservoirs attain saturation levels in all three cases. The lower soil moisture contents give rise to a general decrease in surface runoff rates. The seasonal percentage changes of soil moisture and surface runoff rates for both EB and TG are given in Table 2.

8. Conclusions

A new parameterization of interception is introduced in which the volume of actual interception associated with a given storm is modeled as a function of rainfall intensity, and of an interception capacity that depends on the characteristics of the leaf surface and of the vegetation cover. In addition, the new parameterization accounts for subgrid-scale variability of rainfall intensity and precipitation depth. The resultant formulation is incorporated into the big-leaf and statistical–dynamical

TABLE 2. Percent change of several hydrologic and energy fluxes, between original and modified statistical–dynamical option.

Month	Evergreen broadleaf			Tall grass		
	Rainfall intensity	Soil moisture	Surface runoff rate	Rainfall intensity	Soil moisture	Surface runoff rate
1	22.35	0	−18.74	15.38	0	−7.41
2	14.37	−0.07	−19.05	8.51	0	−7.24
3	18.23	−3.25	−1.41	14.25	−1.44	2.97
4	16.38	−12.68	−2.74	13.3	−7.73	3.86
5	11.68	−19.31	−16.43	10.83	−12.87	−5.14
6	12.43	−22.45	−23.56	13.13	−15.41	−8.91
7	12.42	−23.42	−28.16	11.16	−15.88	−13.5
8	12.78	−22.74	−28.15	11.38	−14.84	−12.14
9	12.41	−21.46	−26.26	10.1	−13.22	−10.99
10	12.82	−20.41	−24.13	8.85	−11.8	−10
11	17.83	−15.06	−52.14	10.92	−5.91	−34.08
12	24.21	−1.13	−31.16	14.74	0	−7.06

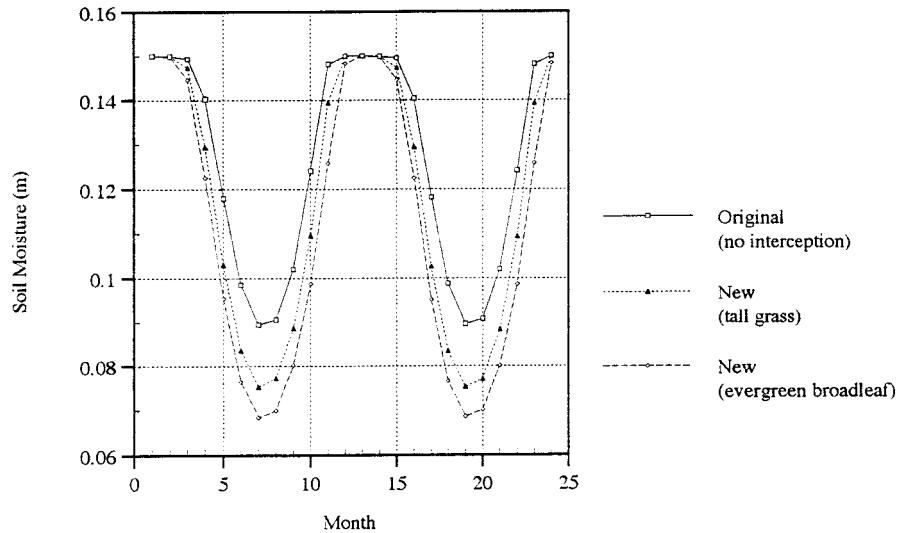


FIG. 8. Seasonal distribution of soil moisture generated with the statistical–dynamical option of the column model.

options of the soil–plant–atmosphere column model of Ramírez. The new interception parameterization has significant impacts on components of the energy and water budgets at the land surface.

By substituting a rain-rate dependent interception capacity parameterization for one that is rain-rate independent, significant increases in runoff and soil moisture, and decreases in evaporation-and-transpiration and rainfall intensity occur. Similarly, by introducing an interception component into a land surface scheme that did not have one before, an increase in precipitation and latent energy flux, and a decrease in runoff and soil moisture content occur. Therefore, the omission or simplified representation of interception in GCM's will give rise to significant uncertainties in climate simulations.

As with all other sensitivity analyses based on column models, the sensitivity of the atmospheric response (e.g., in precipitation) is amplified. Among many other reasons, this amplification results from the absence of a horizontal advection mechanism. Implementation of this scheme in a GCM should produce weaker responses.

9. Final remarks

Fog interception is a significant component of the water budget in high-altitude cloud forests in the Andes, Hawaii, Sri Lanka, etc. (Calder 1992). For example, Cavalier and Goldstein (1989) in studies conducted in three elfin cloud forests in South America have observed total annual rainfall and fog interception estimates of 853 and 796 mm, 1630 and 518 mm, and 4461 and 480 mm for Serrania de Macuira, Guajira, Colombia (865 m); Cerro Santa Ana, Peninsula de Paraguana, Venezuela (815 m); and Cerro Copey, Margarita Island, Venezuela (987 m), respectively. In nontropical climates, snowfall and snowpack also play dominant roles in con-

trolling water fluxes. Therefore, the accurate parameterization of fog and snowfall interception is of importance. The interception parameterization used in this study is valid only for the modeling of the loss of interception capacity due to rain. Furthermore, effects of other storm properties such as rain angle, raindrop size, vegetative properties such as woody area, and wind also should be examined in the context of interception.

Acknowledgments. Partial funding for this work was provided by a grant of the National Institute for Global Environmental Change of the Department of Energy (Grant DE-FC03-90ER61010.) Parts of this work were performed with the support of the Earth Science and Applications Division of NASA Marshall Space Flight Center and the Universities Space Research Association. Supercomputing support was provided by NASA/MSFC and the Global Hydrology and Climate Center in Huntsville, Alabama. The current paper benefitted greatly from comments by Dr. Inez Fung and three other anonymous reviewers.

APPENDIX

Interception Parameterization

Using Eqs. (1a) and (2), the cumulative distribution function (cdf) of interception capacity for the exponential model can be expressed as

$$F_{H_o}(h_o) = \int_{-(1/c) \ln(h_o/a)}^{\infty} \alpha e^{-\alpha i} di = \left(\frac{h_o}{a}\right)^{\alpha/c},$$

$$0 \leq h_o \leq a. \quad (\text{A1})$$

Then, the pdf of interception capacity can be derived as

$$f_{H_o}(h_o) = \frac{\alpha}{ac} \left(\frac{h_o}{a}\right)^{(\alpha/c)-1}, \quad 0 \leq h_o \leq a; \quad \alpha, a, c \geq 0, \quad (A2)$$

whose mean is $E[h_o] = a\alpha/(\alpha + c)$. Using Eqs. (1b) and (2), the cdf for the linear model can be expressed as

$$F_{H_o}(h_o) = \int_{(a-h_o)/b}^{a/b} \alpha e^{-\alpha i} di + \int_{a/b}^{\infty} \alpha e^{-\alpha i} di = [e^{-\alpha(a-h_o)/b} - e^{-\alpha(a/b)}] + e^{-\alpha(a/b)}, \quad 0 \leq h_o \leq a. \quad (A3)$$

The corresponding pdf of interception capacity for the linear model is of the mixed type having a probability mass at the origin and is given by

$$\text{Prob}[H_o = 0] = \int_{a/b}^{\infty} f_i(i) di = e^{-\alpha(a/b)}, \quad h_o = 0$$

$$f_{H_o}(h_o) = \frac{\alpha}{b} e^{-\alpha(a-h_o)/b}, \quad 0 < h_o \leq a, \quad (A4)$$

whose mean is $E[h_o] = [\alpha a/b - 1 + \exp(-\alpha/ba)]/\alpha/b$. The probability mass at the origin represents the finite probability that rainfall intensity exceeds the threshold value of a/b , which reduces the interception capacity to $h_o = 0$.

The actual interception, h_a , is

$$h_a = \begin{cases} h & h < h_o \\ h_o & h \geq h_o \end{cases} \quad (A5)$$

where h is total precipitation depth. A two-parameter gamma density function for precipitation depths is used in this analysis,

$$f_H(h) = \frac{\lambda(\lambda h)^{\kappa-1} e^{-\lambda h}}{\Gamma(\kappa)}, \quad (A6)$$

where the two parameters κ (the shape parameter) and λ are functionally related such that, $\lambda = \kappa/m_H$ (m^{-1}), and m_H is the mean precipitation depth. The symbol, $\Gamma(\cdot)$ in (A6) denotes the complete Gamma function, defined as

$$\Gamma(\kappa) = \int_0^{\infty} h^{\kappa-1} e^{-h} dh \quad (A7)$$

The spatial average of the actual interception can be defined using the following integral relationship:

$$E[h_a] = \int_0^{\infty} E[h_a|h_o] f_{H_o}(h_o) dh_o, \quad (A8)$$

where

$$E[h_a|h_o] = \int_0^{\infty} h_a f_{H_a|H_o}(h_a|h_o) dh_a = \int_0^{h_o} \frac{\lambda h_a (\lambda h_a)^{\kappa-1} e^{-\lambda h_a}}{\Gamma(\kappa)} dh_a + h_o [1 - P(\kappa, \lambda h_o)], \quad (A9)$$

which can be simplified to

$$E[h_a|h_o] = \frac{\kappa}{\lambda} P(\kappa + 1, \lambda h_o) + h_o [1 - P(\kappa, \lambda h_o)]. \quad (A10)$$

In Eq. (A9), $f_{H_a|H_o}(h_a|h_o)$ is the conditional pdf of h_a given h_o , which is of the mixed type and has a probability mass at $h_a = h_o$ representing the probability that a given storm will produce a total precipitation depth exceeding the interception capacity and thus resulting in actual interception equaling the interception capacity. The expression $P(\cdot, \cdot)$ in (A9) is Pearson's complementary Gamma function defined as

$$P(\kappa, \lambda h_o) = \frac{\int_0^{h_o} \lambda (\lambda h_a)^{\kappa-1} e^{-\lambda h_a} dh_a}{\Gamma(\kappa)} = \frac{\gamma(\kappa, \lambda h_o)}{\Gamma(\kappa)}, \quad (A11)$$

where $\gamma(\kappa, \lambda h_o)$ is the incomplete Gamma function as defined by the numerator of (A11).

The pdf of interception capacity, $f_{H_o}(\cdot)$ in (A8) depends on whether the linear or the exponential model is used for interception capacity. For each of these two modeling options, (A8) leads to the following results:

$$E[h_a] = \int_0^a \left\{ \frac{\kappa}{\lambda} P(\kappa + 1, \lambda h_o) + h_o [1 - P(\kappa, \lambda h_o)] \right\} \frac{\alpha}{ac} \left(\frac{h_o}{a}\right)^{(\alpha/c)-1} dh_o, \quad (A12)$$

$$E[h_a] = \int_0^a \left\{ \frac{\kappa}{\lambda} P(\kappa + 1, \lambda h_o) + h_o [1 - P(\kappa, \lambda h_o)] \right\} \frac{\alpha}{b} e^{-[\alpha(a-h_o)]/b} dh_o. \quad (A13)$$

As functions of the normalized actual interception $h_a^* = h_a/a$, and of the normalized interception capacity $h_o^* = h_o/a$, Eqs. (A13) and (A14) can be rewritten as

$$E[h_a^*] = \int_0^1 \left\{ \eta P\left(\kappa + 1, \frac{\kappa h_o^*}{\eta}\right) + h_o^* \left[1 - P\left(\kappa, \frac{\kappa h_o^*}{\eta}\right) \right] \right\} \tau h_o^{*(\tau-1)} dh_o^* \quad (\text{A14})$$

for the exponential model, and as

$$E[h_a^*] = \int_0^1 \left\{ \eta P\left(\kappa + 1, \frac{\kappa h_o^*}{\eta}\right) + h_o^* \left[1 - P\left(\kappa, \frac{\kappa h_o^*}{\eta}\right) \right] \right\} v e^{-v(1-h_o^*)} dh_o^* \quad (\text{A15})$$

for the linear model, respectively. The climate vegetation parameter $\eta = \kappa/(\lambda a)$ is equal to the ratio of mean precipitation depth to maximum dew depth. Here $\tau = 1/E(i)c = \alpha/c$, and $v = (a/b)/E(i) = \alpha a/b$ are the normalized interception capacity decay parameters for the exponential and linear models, respectively.

REFERENCES

- Aston, A. R., 1979: Rainfall interception by eight small trees. *J. Hydrol.*, **42**, 383–396.
- Bultot, F., G. L. Dupriez, and A. Bodeux, 1972: Interception de la pluie par la végétation forestière: Estimation de l'interception journalière à l'aide d'un modèle mathématique. *J. Hydrol.*, **17**, 193–223.
- Calder, I. R., 1977: The model of transpiration and interception loss from a spruce forest in Plynlimon, central Wales. *J. Hydrol.*, **33**, 247–265.
- , 1992: Hydrological effects of land-use change. *Handbook of Hydrology*, D. R. Maidment, Ed., McGraw-Hill, 13.1–13.50.
- Cavelier, J., and G. Goldstein, 1989: Mist and fog interception in elfin cloud forests in Colombia and Venezuela. *J. Tropical Ecol.*, **5**, 309–322.
- Crockford, R. H., and D. P. Richardson, 1990: Partitioning of rainfall in a eucalypt forest and pine plantation in southeastern Australia. IV: The relationship of interception and canopy storage capacity, the interception of these forests, and the effects on interception of thinning the pine plantation. *Hydrol. Proc.*, **4**, 169–188.
- Deardorff, J., 1978: Efficient prediction of ground temperature and moisture with inclusion of a layer of vegetation. *J. Geophys. Res.*, **83**, 1889–1903.
- Dickinson, R. E., and A. Henderson-Sellers, 1988: Modeling tropical deforestation: A study of GCM land-surface parameterizations. *Quart. J. Roy. Meteor. Soc.*, **114**, 439–462.
- , —, P. J. Kennedy, and M. F. Wilson, 1986: Biosphere–Atmosphere Transfer Scheme (BATS) for the NCAR Community Climate Model. NCAR Tech. Note NCAR/TN-275 + STR, 80 pp.
- Eagleson, P. S., 1978: Climate, soil and vegetation. Part II: The distribution of annual precipitation derived from observed storm sequences. *Water Resour. Res.*, **14**, 5, 713–721.
- Eltahir, E. A. B., and R. L. Bras, 1993: A description of rainfall interception over large areas. *J. Climate*, **6**, 1002–1008.
- Entekhabi, D., and P. S. Eagleson, 1989: Land surface hydrology parameterization for atmospheric general circulation models including subgrid scale spatial variability. *J. Climate*, **2**, 816–831.
- Franken, W., P. R. Leopoldo, E. Matsui, and M. N. G. Ribeiro, 1982: Intreceptação das precipitações em floresta Amazônica de terra firme. *Acta Amazon.*, **12**, 15–122.
- Hancock, N. H., and J. M. Crowther, 1979: A technique for the direct measurement of water storage on a forest canopy. *J. Hydrol.*, **41**, 105–122.
- Hawk, K. L., and P. S. Eagleson, 1992: Climatology of station storm rainfall in the continental United States: Parameters of the Bartlett-Lewis and Poisson rectangular pulses models. MIT Parsons Laboratory TR No. 336, 330 pp.
- Helvey, J. D., and J. H. Patric, 1965: Canopy and litter interception of rainfall by hardwoods of eastern United States. *Water Resour. Res.*, **1**, 193–206.
- Horton, R. E., 1919: Rainfall interception. *Mon. Wea. Rev.*, **47**, 603–623.
- Ison, N. T., A. M. Feyerherm, and L. D. Bark, 1971: Wet period precipitation and the gamma distribution. *J. Appl. Meteor.*, **10**, 658–665.
- Jackson, I. J., 1975: Relationships between rainfall parameters and interception by tropical forest. *J. Hydrol.*, **24**, 215–238.
- Koster, R. D., and P. C. D. Milly, 1997: The interplay between transpiration and runoff formulations in land surface schemes used with atmospheric models. *J. Climate*, **10**, 1578–1591.
- Lean, J., and D. A. Warrilow, 1989: Simulation of the regional impact of Amazon deforestation. *Nature*, **342**, 411–413.
- Lee, T. J., 1992: The impact of vegetation on the atmospheric boundary layer and convective storms. Ph.D. dissertation, Colorado State University, 137 pp.
- Mahfouf, J., and B. Jacquemin, 1989: A study of rainfall interception using a land surface parameterization for mesoscale meteorological models. *J. Appl. Meteor.*, **28**, 1282–1302.
- Massman, W. J., 1980: Water storage on forest foliage: A general model. *Water Resour. Res.*, **16**, 210–216.
- , 1983: The derivation and validation of a new model for the interception of rainfall by forests. *Agric. Meteor.*, **28**, 261–286.
- Ramírez, J. A., 1991: The role of atmosphere/surface interactions in global and regional hydrologic cycles. *Proc. 11th Annual American Geophysical Union Hydrology Days Publications*, Fort Collins, CO, Amer. Geophys. Union, 47–58.
- , and R. L. Bras, 1985: Conditional distributions of Neyman-Scott Models for storm arrivals and their use in irrigation scheduling. *Water Resour. Res.*, **21**, 765–776.
- , and A. M. Genovez, 1994: Sensitivity analysis and inter comparison of global hydrologic cycles obtained with different land surface on schemes. *Proc. Sixteenth Latin American Congress in Hydraulics*, Santiago de Chile, Chile, International Association for Hydraulic Research, 157–168.
- Sellers, P. J., Y. Mintz, Y. C. Sud, and A. Dalcher, 1986: A Simple Biosphere Model (SiB) for use within general circulation models. *J. Atmos. Sci.*, **43**, 505–531.
- , F. G. Hall, G. Asrar, D. E. Strebel, and R. E. Murphy, 1988: The First ISLSCP Field Experiment (FIFE). *Bull. Amer. Meteor. Soc.*, **69**, 22–27.
- , W. J. Shuttleworth, J. L. Dorman, A. Dalcher, and J. M. Roberts, 1989: Calibrating the Simple Biosphere model for Amazonian

- tropical forest using field and remote sensing data. Part I: Average calibrating with field data. *J. Appl. Meteor.*, **28**, 727–759.
- , D. A. Randall, C. J. Collatz, J. A. Berry, C. B. Field, D. A. Dazlich, C. Zhang, and G. D. Collelo, 1996: A revised land surface parameterization (SiB2) for Atmospheric GCMs. Part 1: Model formulation. *J. Climate*, **9**, 676–705.
- Shuttleworth, W. J., 1988: Evaporation from Amazonian rainforest. *Proc. Roy. Soc. London, Ser. B*, **233**, 321–346.
- Trimble, G. R., Jr., and S. Weitzman, 1954: Effect of a hardwood forest canopy on rainfall intensities. *Amer. Geophys. Union Trans.*, **35**, 226–234.
- Wells, L. P., and G. J. Blake, 1972: Interception characteristics of some central North Island vegetation and their geographical significance. *Proc. Seventh New Zealand Geogr. Conf.*, Hamilton, New Zealand, 217–224.
- Williamson, D. L., J. T. Kiehl, V. Ramanathan, R. E. Dickinson, and J. J. Hack, 1987: Description of NCAR Community Climate Model (CCM1). NCAR Tech. Note NCAR/TN-285 + STR, 112 pp.
- Zinke, P. J., 1967: Forest interception studies in the United States. *International Symposium on Forest Hydrology*, W. E. Sopper and H. W. Hull, Eds., Pergamon Press, 823 pp.